Advanced Powder Technology 35 (2024) 104460

Contents lists available at ScienceDirect

Advanced Powder Technology

journal homepage: www.elsevier.com/locate/apt

Fabrication of g-C_3N_4 films with enhanced mechanical and charge transfer properties by electrophoretic deposition and subsequent citric acid modification

Preyaphat Wongchaiya [a,b], Thi Kim Ngan Nguyen [c,*], Pornapa Sujaridworakun [a,d,e,*], Siriporn Larpkiattaworn [f], Tohru S. Suzuki [b], Tetsuo Uchikoshi [b,*]

[a] Department of Materials Science, Faculty of Science, Chulalongkorn University, 254 Phayathai Road, Pathumwan, Bangkok 10330, Thailand
[b] Research Center for Electronic and Optical Materials, National Institute for Materials Science, 1-2-1 Sengen, Tsukuba, Ibaraki 305-0047, Japan
[c] International Center for Young Scientists, National Institute for Materials Science, 1-2-1 Sengen, Tsukuba, Ibaraki 305-0047, Japan
[d] Photocatalysts for Clean Environment and Energy Research Unit, Faculty of Science, Chulalongkorn University, 254 Phayathai Road, Pathumwan, Bangkok 10330, Thailand
[e] Center of Excellence on Petrochemical and Materials Technology, Chulalongkorn University, 254 Soi Chula 12, Phayathai Road, Wang Mai, Pathumwan, Bangkok 10330, Thailand
[f] Expert Centre of Innovative Materials, Thailand Institute of Scientific and Technological Research, 35 Mu 3 Technopolis, Tambon Khlong Ha, Amphoe Khlong Luang, Pathum Thani 12120, Thailand

ARTICLE INFO

Article history:
Received 30 January 2024
Received in revised form 16 April 2024
Accepted 24 April 2024
Available online xxxx

Keywords:
Graphitic carbon nitride
Citric acid
Electrophoretic deposition
Chemical interaction
Optoelectronic device

ABSTRACT

A low-cost 2D metal-free material based on a graphitic carbon nitride (g-C_3N_4) film functionalized with a citric acid molecule has been successfully fabricated by Electrophoretic Deposition (EPD) and thermal techniques, aiming to evaluate its suitability for optoelectronic devices. The thickness-controlled g-C_3N_4 film having a good mechanical property was successfully performed. The chemical stability and photostability of the citric-modified g-C_3N_4 films deposited on indium tin oxide (ITO) glass were investigated. New chemical links were clarified such that it could possibly become a bridge for enhancing charge transport. The modified samples exhibited a significant increase in their photocurrent response, reaching 25 μA/cm^2 at a thickness of about 20 μm. Electrochemical impedance spectra (EIS) verified the enhanced conductivity, efficient charge transfer, and reduced electron-hole recombination rate. This research revealed a facile synthetic route and environmentally benign materials, thereby suggesting promising prospects for their application in the optoelectronic field.

1. Introduction

Global warming has prompted research on optoelectronic materials for renewable energy. Their versatile applications in solar cells, lighting, energy storage, and greenhouse gas monitoring have addressed urgent environmental challenges [1,2]. However, commonly used optoelectronic materials, such as GaAs, InAS, CdSe, PbS, and InSb [3–7], have the following drawbacks: high cost, scarcity, and potential environmental and social concerns linked to their extraction and mining processes. The metal-free semiconductor known as graphitic carbon nitride (g-C_3N_4) has garnered significant attention within the optoelectronics field due to its distinctive attributes. Possessing a robust thermal and chemical stability along with an optimal bandgap for effective visible light absorption, g-C_3N_4 has emerged as a standout candidate. Moreover, its cost-effectiveness and synthesis feasibility using abundant, eco-friendly elements, make it an attractive semiconductor alternative [8,9]. The g-C_3N_4 has demonstrated its effectiveness as a photocatalyst for water splitting, pollutant degradation, and hydrogen production. Moreover, its utility extends to areas such as photovoltaics, gas sensing, and energy storage systems [10–13]. Nevertheless, the majority of bulk g-C_3N_4 application remains constrained by its low surface area, high electron-hole pair recombination rates, and limited charge transfer propensity [14]. To overcome these issues, various approaches are employed, including morphological modifications [15], elemental doping [16], and the fabrication of g-C_3N_4-based heterostructures [17]. Furthermore, chemical functionalization via covalent or noncovalent interactions is extensively acknowledged and utilized methodologies for tailoring the g-C_3N_4 properties [18]. Vidyasagar et al. [19]

* Corresponding authors at: Department of Materials Science, Faculty of Science, Chulalongkorn University, 254 Phayathai Road, Pathumwan, Bangkok 10330, Thailand (P. Sujaridworakun).
E-mail addresses: NGUYEN.Thikimngan@nims.go.jp (T.K.N. Nguyen), pornapa.s@chula.ac.th (P. Sujaridworakun), uchikoshi.tetsuo@nims.go.jp (T. Uchikoshi).

https://doi.org/10.1016/j.apt.2024.104460
0921-8831/

employed a post-functionalization approach to introduce the 2,5-thiophene dicarboxylic acid (TDA) moiety into the defect sites of g-C_3N_4. Within the electronic structure of g-C_3N_4-TDA, an electron-accepting —C═O thiophene segment is linked to the g-C_3N_4 unit via an amide (—NH—C═O). This configuration enhances the interfacial charge transfer and fosters efficient separation of the charge carriers, significantly contributing to its heightened photocatalytic performance. However, in its powdered form, its range of applications is constrained.

Fabricating g-C_3N_4 films is vital due to their non-self-standing nature, requiring substrates or supports for shape maintenance. Despite common methods, such as dip coating [20], drop-casting [21], and spin coating [22], the films exhibit an unpredictable thickness and low photocurrent response. On the other hand, techniques, such as chemical vapor deposition (CVD) [23] and atomic layer deposition (ALD) [24], offer precise control over the deposition process. However, these methods can be complex and expensive. They may not be suitable for large-scale production. The electrophoretic deposition (EPD) method is preferred for fabricating g-C_3N_4 films due to its exceptional ability to precisely deposit g-C_3N_4 particles onto a substrate, allowing for a controlled thickness. This technique involves the application of an electric field to force charged g-C_3N_4 sheets within a suspension toward the electrode, resulting in their controlled and targeted deposition onto the substrate [25]. Han et al. recently synthesized porous nanosheets of g-C_3N_4 using glyoxal-treated melamine as a precursor and fabricated their films on fluorine-doped tin oxide (FTO) substrates by EPD. Remarkably, the porous g-C_3N_4 nanosheets exhibited a significant photocatalytic activity for photodegradation of isopropyl alcohol (IPA) and gaseous nitric oxide (NO). Notably, their photocurrent density reached 3.5 μA/cm^2, surpassing the value of 0.76 μA/cm^2 observed for g-C_3N_4 films [26]. In addition, Phoon et al. fabricated mesoporous graphitic carbon nitride (GCN) films by using EPD that showed a high efficiency in photodegrading tetracycline (TC) antibiotics and exhibited a photocurrent response of about 2 μA/cm^2 [27]. However, the photocurrent response of the g-C_3N_4 films remains relatively low, as indicated by studies [28–30], attributed to deficient adhesion between the g-C_3N_4 and ITO glass, resulting in detachment during electrochemical analyses. Thus, organic molecule modification of the g-C_3N_4 films becomes essential for improving adhesion and fostering a surface charge transfer, charge separation, and reduced carrier recombination rates.

Citric acid ($C_6H_8O_7$), a natural organic polycarboxylic acid with three carboxyl groups, is commonly employed as a non-toxic and cost-effective precursor. It serves as cross-linker agents [31], disinfectant, environmental remediation [32], and sterilizing agents [33,34]. Studies have investigated its potential as a cross-linker agent to enhance the physical and mechanical properties of materials like cellulose [35], starch [36], and wood [37]. Furthermore, citric acid (CA) serves as a reagent, either alone or most frequently in combination with nitrogen-containing compounds, for the synthesis of Carbon Dots (C-dots). This process yields C-dots with diverse structures and optical properties [38].

In this study, the g-C_3N_4 powder was synthesized by the pyrolysis of urea [39]. Subsequently, a g-C_3N_4 film was fabricated on ITO glass by the EPD method using a dispersing medium of acetone and iodide. The study aims to enhance adhesion between the g-C_3N_4 and ITO substrates along with improving the surface charge transfer and photocurrent response. This is achieved by functionalizing g-C_3N_4 films with citric acid moieties and optimizing the synthetic conditions. The results of this study show that modification with citric acid improves the physical stability and photoelectric conversion properties of g-C_3N_4 films prepared by the EPD method, which is important information for optoelectronic device applications.

2. Material and methods

2.1. Synthesis of g-C_3N_4

The g-C_3N_4 powder was prepared by the simple pyrolysis of urea (98 %, Sigma-Aldrich). In the procedure, a total of 10.0 g of urea powder was weighed, then placed in an alumina crucible with an outer diameter of 46 mm and height of 36 mm, which was subsequently covered. The crucible was subjected to heating in an electric furnace (Koyo Thermo Systems Co., Ltd., Japan) at the rate of 5.0 °C/min in the presence of air, reaching a temperature of 550 °C, and maintained at this temperature for 4 h. After the completion of the heating process, the resulting product had a pale-yellow color. The BET specific surface area of the synthesized g-C_3N_4 powder was 86.9 m^2/g.

2.2. Electrophoretic deposition of g-C_3N_4 layer on ITO glass

The g-C_3N_4 layer was fabricated on an ITO glass substrate using the EPD method. A schematic diagram of the fabrication of CA-modified g-C_3N_4 film by EPD and subsequent thermal process is shown in Fig. 1. To ensure stable suspensions, 0.5 g of g-C_3N_4 powder was dispersed in 50 ml of acetone (Nacalai Tesque, Inc., Japan) and subjected to ultrasonication for 1 h using an ultrasonication homogenizer. Subsequently, a 100 μl solution of iodine (ACS grade 99.5 %, Sigma-Aldrich), used as an effective dispersant agent for electrostatic stabilization in EPD suspensions and to induce a positive surface charge on the g-C_3N_4 particles, was added to the slurry. The sonication process was then continued for an additional 20 min. The zeta potential of g-C_3N_4 changed from −6.56 mV to +34.4 mV with the addition of iodine. The particle size of g-C_3N_4 ranged from 0.5 to 4 μm with and without the addition of iodine. For the deposition process, an ITO glass substrate with an area of 2 × 3 cm^2 (Geomatec Co., Ltd., Japan; 6.15–7.27 Ohm/sq) was employed as the cathode (deposition electrode), while a stainless-steel sheet was used as the anode (counter electrode), with a fixed distance of 10 mm maintained between the two electrodes. Based on preliminary investigations, the optimal conditions for the EPD method were determined. A potential of 25 V was applied across the electrodes, and the deposition was carried out for a duration of 10 s. Finally, the coated samples were dried in an oven at 50 °C for one hour to ensure complete evaporation of the solvent and achieve a uniform g-C_3N_4 layer on the ITO glass substrate.

2.3. Surface modification of g-C_3N_4 layer with citric acid

Citric acid (98 %, FUJIFILM Wako Pure Chemical Industries, Ltd., Japan) was dissolved in acetone (CH_3COCH_3, Nacalai Tesque, Inc., Japan) to prepare solutions with various concentrations of 10, 25, 50, 75, and 100 g/l. Subsequently, 80 μl of these citric acid solutions were drop onto the as-prepared g-C_3N_4 layer on the ITO glass substrate. The samples were then placed on a hot plate and heated at 120 °C for a duration of 1 h to allow for solvent evaporation and enhance adhesion between the citric acid and g-C_3N_4. Following the initial heating step, the samples underwent a further heat treatment at temperatures of 200 °C, 250 °C, 300 °C, and 350 °C for an additional 2 h. This extended heat treatment aimed to induce specific changes or reactions in the citric acid-g-C_3N_4 system, and to study the temperature-dependent effects on the resulting material. The prepared g-C_3N_4-CA samples, heated at 300 °C and modified with a citric acid concentration of 50 g/L, were labeled as follows: g-C_3N_4-CA-300 °C and g-C_3N_4-CA 50 g/l, respectively, based on the heating temperature and citric acid concentration used in the fabrication process.

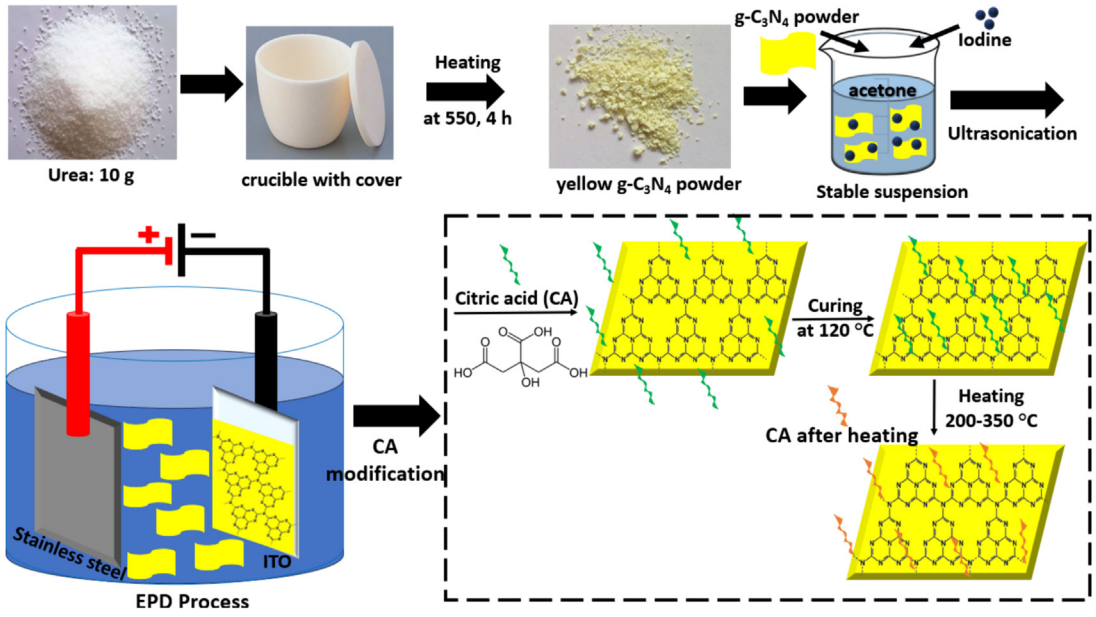

Fig. 1. Schematic overview of CA modified g-C_3N_4 film fabrication via thermal process.

2.4. Measurement of photocurrent response

Photocurrent measurements were performed using an electrochemical analyzer (VSP-300 Potentiostat, BioLogic Science Instruments, France). The experimental setup consisted of a standard three-electrode cell, in which the prepared samples served as the working electrode, a Pt sheet acted as the counter electrode, and an Ag/AgCl electrode functioned as the reference electrode. A 0.1 M Na_2SO_4 (Wako Pure Chemical Industries, Ltd., Japan) aqueous solution was used as the electrolyte. The applied potential was 1.23 V, and the active area of the working electrode was 4 cm^2. To generate light illumination, a 300 W compact Xenon light source (MAX-303, Asahi Spectra Co., Ltd., Japan), positioned 10 cm from the reactor, was utilized. The electrochemical impedance spectroscopy (EIS) was performed using a potentiostat. The Nyquist plots were measured at 1.23 V (vs. Ag/AgCl) with an AC amplitude of 10 mV, frequency of 0.01–100,000 Hz under a 300 W compact Xenon light source.

2.5. Characterization

The morphology of the samples was characterized using a Field Emission Scanning Electron Microscope (FE-SEM, S-4800, Hitachi High-Tech Corporation) operated at an acceleration voltage of 5 kV. To analyze the crystal structure of the samples, X-ray Diffraction (XRD) patterns were measured at room temperature using a Grazing Incidence X-ray Diffractometer (GI-XRD, Rigaku Corporation, Japan). The measurements were conducted in the 2-theta angle range of 10–45°, utilizing Cu Kα radiation (λ = 1.5418 Å) at 45 kV, 200 mA. The step size for the scans was set at 0.02° with a scan speed of 1°/min, and the incident angle was set to 0.5°. The chemical bonding in the samples was investigated using a Fourier Transform Infrared Spectrometer (FT/IR-4100, Jasco International Co., Ltd., Japan). The samples were analyzed in the wavenumber range of 400–4000 cm^{-1}, which allowed for identification of the characteristic vibrational modes associated with different chemical bonds. To measure the absorbance properties of the films, a UV–Vis spectrophotometer (V-650, Jasco International Co., Ltd., Japan) was employed. The measurements were carried out in the wavelength range of 200–800 nm at the scan rate of 400 nm/min. The luminescence spectra of the samples were recorded at room temperature using a NanoLog spectrofluorometer (HORIBA Instruments Incorporated, Japan) equipped with a 450 W xenon arc lamp. The excitation wavelength was 370 nm, and the emitted light was measured to analyze the luminescent properties of the samples. Additionally, the binding energy of the samples was determined using X-ray Photoelectron Spectroscopy (XPS) by a PHI Quantera SXM instrument (Ulvac-PHI) employing Al Kα radiation at 15 kV. The binding energies were calibrated with respect to the C1s peak of the adventitious carbon at 285 eV. This technique provided information about the chemical state and electronic structure of the samples.

3. Results and discussion

FE-SEM images were employed to analyze the morphology and microstructure of the g-C_3N_4, and g-C_3N_4-CA films deposited on the ITO glass. Fig. 2 displays the SEM images corresponding to different heating conditions during the film fabrication process. The SEM images of the g-C_3N_4 film (Fig. 2**a**) and the g-C_3N_4-CA film (Fig. 2**b**) show a slightly aggregated structure with two-dimensional sheet-like formations that have irregular edges and slight curls. These sheets are extremely thin, measuring only a few nanometers in thickness, and a range in size from tens to hundreds of nanometers. The images also highlight the high porosity of the films. When the g-C_3N_4-CA film undergoes additional heat treatment at 200 °C and 300 °C (Fig. 2**c and d**, respectively), there was no noticeable change in the particle shape and size by the acid treatment, indicating that the presence of citric acid has a minimal impact on the microstructures of the g-C_3N_4, as observed in the images. Additionally, Fig. 2**e and f** show a cross-section view of the g-C_3N_4 and g-C_3N_4-CA-300 °C films on the ITO glass, respectively, revealing a film thickness of 28 μm for g-C_3N_4 film. However, the reduction of the thickness to about 20 μm was observed after the induced citric acid and heating process. The thermal treatment released adsorbed solvent molecules, creating cross-linking between the citric acid and g-C_3N_4. The film thickness plays a pivotal role in the generation and transportation of charge carriers [40], subsequently influencing the photocurrent response. Nevertheless, although the photocurrent magnitude rises with the

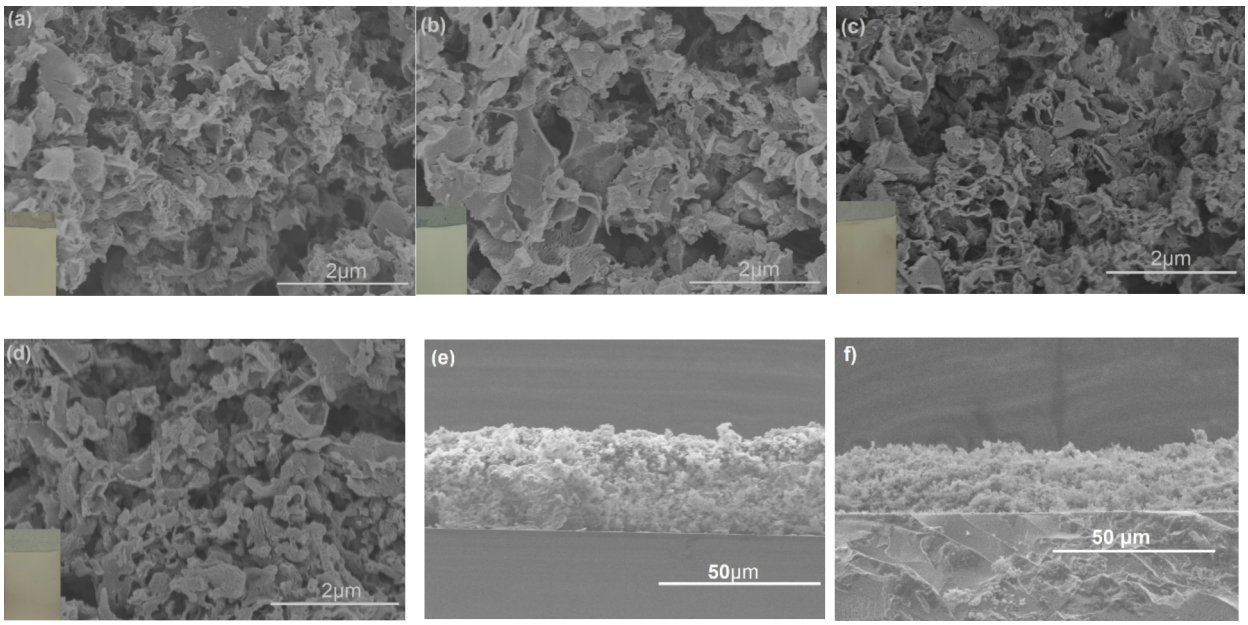

Fig. 2. FE-SEM images of EPD films containing a) g-C_3N_4 and b) g-C_3N_4-CA c) g-C_3N_4-CA 200 °C d) g-C_3N_4-CA 300 °C, Cross-section of e) g-C_3N_4 f) g-C_3N_4-CA-300 °C, with a constant CA concentration of 75 g/l.

thicker films, excessively thick films during the electrochemical measurements can lead to detachment from the ITO substrate. Thus, determining the optimum film thickness is critical.

The X-ray diffraction (XRD) analysis of the g-C_3N_4 film on the ITO glass revealed two prominent diffraction peaks at 2θ of 13.0° and 27.4°, which align with the JCPDS 87-1526 database (Fig. 3) [41]. The peak observed at 2θ = 13.0° corresponds to the (100) crystal plane of g-C_3N_4, indicating the in-plane structural arrangement. The strong peak at 2θ = 27.4° corresponds to the (002) crystal plane of g-C_3N_4, representing the characteristic interlayer stacking structure. The X-ray diffraction (XRD) pattern of g-C_3N_4-CA without additional heat treatment shows clear peaks that correspond to citric acid (CA). The indication of the characteristic XRD peaks confirms the presence of CA in the sample. When the g-C_3N_4-CA sample was heated to 200 °C on higher, an unidentified phase occurred. This occurrence could be attributed to the potential melting of the citric acid and its interaction with the g-C_3N_4 phase or transformation into another form. To understand the changes that the citric acid underwent during heating from 200 °C to 350 °C, please refer to **Fig. S1**, which illustrates the melting of citric acid and the formation of an amorphous phase, as indicated by the broad peak observed in Fig. S1**a**. Furthermore, in Fig. S1**b**, the sample exhibited an apparent gel-like appearance and a high degree of stickiness at 200 °C. At 250 °C, it transformed into a fine powder with a brownish texture. Finally, at 300 °C and 350 °C, the sample transitioned into coarse particles with a black coloration. The thermal decomposition of citric acid is a multi-step process leading to the formation of intermediate products like *trans*-aconitic acid and citraconic anhydride [42,43]. Citric acid initially melts at 153 °C, followed by dehydration at 175 °C, resulting in aconitic acid. As the temperature continues to rise, decarboxylation reactions occur, yielding methyl maleic anhydride or citraconic anhydride [44]. These intermediates, formed during the decomposition process, may subsequently undergo chemical interactions with the g-C_3N_4 material during the heat treatment. These interactions have the potential to induce unknown peaks in the crystallographic structure of the sample due to the thermal treatment.

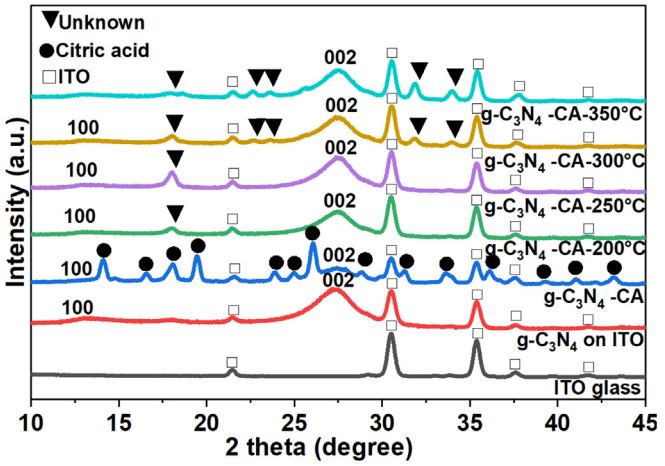

Fig. 3. X-ray diffraction (XRD) patterns of the films on ITO glass obtained at different calcination temperatures with a constant CA concentration of 75 g/l.

The FTIR spectra presented in Fig. 4**a** reveals the chemical bonding vibrations of pure citric acid (CA), pure g-C_3N_4, and g-C_3N_4-CA films with various CA concentrations without additional heat treatment. The results showed that the g-C_3N_4-CA film at a concentration of 10 g/L exhibited a lower intensity peak corresponding to CA. Concentrations exceeding this value distinctly showed the presence of the CA peak in the g-C_3N_4 matrix. In Fig. 4**b**, the spectra of the pure CA heated at 300 °C, g-C_3N_4 and g-C_3N_4-CA films heated at 200–350 °C were analyzed. In the spectra, multiple absorption peaks were observed in the range of 1200–1640 cm^{-1}, which can be attributed to the stretching vibrations of C-N and C=N bonds present in the CN aromatic repeating units of the g-C_3N [45]. Furthermore, absorption peaks at 810 cm^{-1} indicated the characteristic out-of-plane vibrations of the triazine/s-triazine aromatic repeating units [46]. Moreover, the FTIR spectra of the g-C_3N_4-CA-200 to 350 °C samples showed the presence of peaks associated with g-C_3N_4. However, the peak corresponding to citric acid (CA) is not clearly observed, suggesting that the CA component may have undergone some changes or reactions during the heating process.

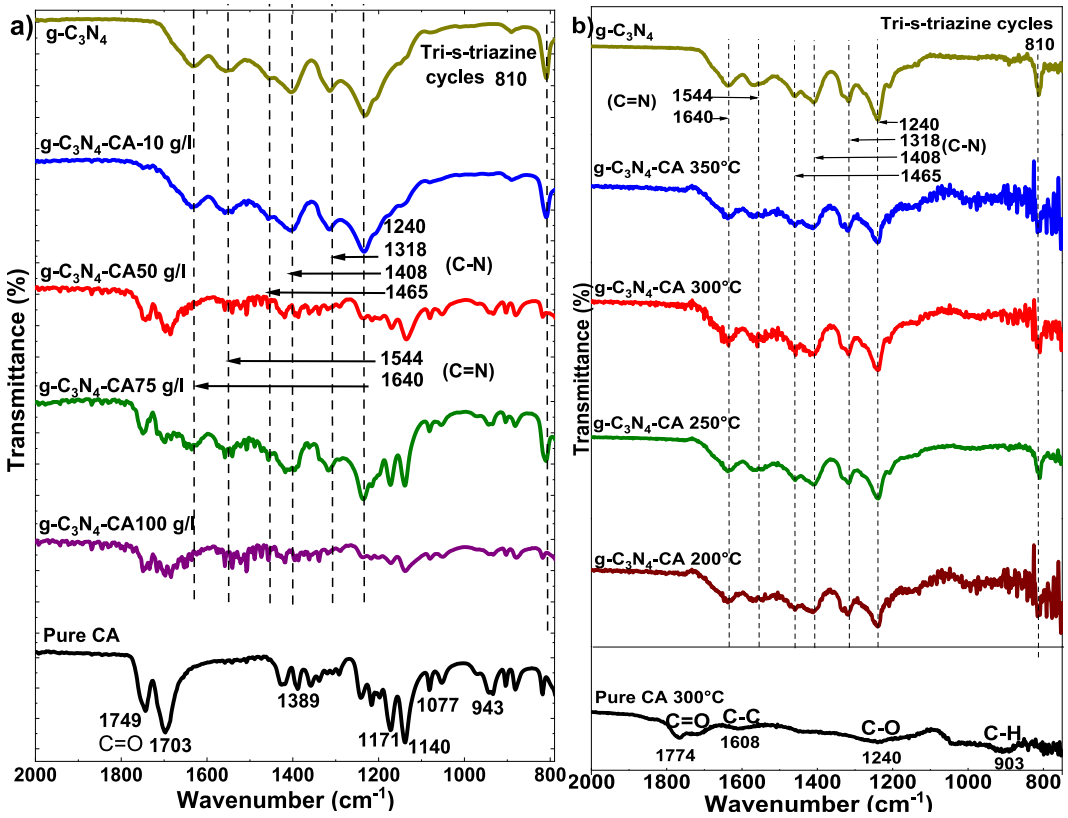

Fig. 4. FTIR of g-C_3N_4 and g-C_3N_4-CA on ITO glass obtained at a) by varying the CA concentration, without additional heat treatment, and b) various calcination temperatures at 200–350 °C.

To gain further insight into the transformation of citric acid, the FTIR spectrum of pure citric acid heated at 300 °C (**Fig. S2**) was examined. Comparing the FTIR absorption spectra within the 1900–1600 cm^{-1} range of citric acid (CA) before and after heating, distinctive changes were observed. The two C═O stretching bands in the FTIR spectrum of the pure citric acid (Fig. 4**a**), located at 1749 and 1703 cm^{-1}, exhibit a different relative intensity and shift with respect to CA-300 °C (**Fig. S2**). These findings are consistent with observations made in a previous study [47], highlighting intense absorption bands characteristic of citraconic anhydride at 1774 cm^{-1} (C═O stretching of anhydride carbonyl) and 1844 cm^{-1} (C═O antisymmetric stretching). This suggests that, after heating, the citric acid component likely transforms into itaconic or/and citraconic anhydride [43]. These anhydrides possess a carbonyl group that can potentially form a covalent bond with the N-atom of g-C_3N_4. The introduction of the —C═O moiety connected to the g-C_3N_4 unit via an amide (—NH—C═O) linkage plays a pivotal role in augmenting charge separation between electrons and holes, thereby improving the light absorption properties and improving the photocurrent response.

The X-ray photoelectron spectroscopy (XPS) analysis of g-C_3N_4 and g-C_3N_4-CA-300 °C provided information about the surface composition and bonding of these materials. In the high-resolution C 1s spectrum (Fig. 5**a**) of g-C_3N_4, two distinct carbon bonding states were observed. The peak observed at 284.9 eV can be attributed to the C—C bond of the surface adventitious carbon. On the other hand, the peak at 288.3 eV indicated the presence of sp^2-bonded carbon (N—C═N) [48]. For the g-C_3N_4-CA-300 °C, the C1s binding energies could be fitted to four peaks. Two prominent peaks appeared at 286.2 and 288.0 eV, which can be attributed to the C—O and C═O bonds, respectively [49]. **Figure S3** illustrates the comparative XPS spectra of g-C_3N_4 and g-C_3N_4-CA-300 °C, both exhibiting similar overall features. However, a notable difference is observed in the ratio of the peak height at 288.3 eV to that at 285.0 eV between the two samples. Specifically, the peak height ratio for g-C_3N_4 is 12:1, whereas for g-C_3N_4-CA-300 °C, this ratio is 3:1. This significant change in the peak height ratio indicated that g-C_3N_4-CA-300 °C contains a concentration of C—C functional groups that is four times higher compared to the pure g-C_3N_4. The increase in the number of C—C bonds can be attributed to the presence of citric acid during the modification of g-C_3N_4-CA-300 °C. In the O1s spectra (Fig. 5**b**) of g-C_3N_4, two main peaks were observed. These corresponded to the external —OH group or water molecules adsorbed on the surface and N—O bonds at 531.9 eV and 533.1 eV, respectively [50]. Interestingly, a new peak appeared at 532.2 eV for the g-C_3N_4-CA-300 °C, which can be attributed to the formation of the C═O species, indicating a chemical change caused by heating the material with citric acid. By analyzing the N 1s spectrum (Fig. 5**c**), four fitted peaks were observed for g-C_3N_4, corresponding to different nitrogen species. The binding energies of these peaks were measured at 398.6 eV, 399.1 eV, 401.0 eV, and 404.6 eV. These peaks can be attributed to C—N═C (sp^2-hybridized nitrogen), N—C_3 (sp^3-hybridized nitrogen), C—N—H (amino group from the surface uncondensed bridging N atom), and the π–π* excitations between the stacking interlayers, respectively [51]. Regarding the g-C_3N_4-CA-300 °C, there was a peak shift to 400.6 eV compared to the pristine g-C_3N_4 at 401.0 eV. This decrease in binding energy indicated a shift towards lower energies corresponding to the N— (C═O) bond, suggesting that, after heating at 300 °C, an interaction occurred between the citric acid and g-C_3N_4. The disparities observed in the XPS data between the g-C_3N_4 and g-C_3N_4-CA-300 °C provided evidence that, after heating at 300 °C, the carbonyl (C═O) groups of citric acid can form bonds with the NH_2 group of the triazine

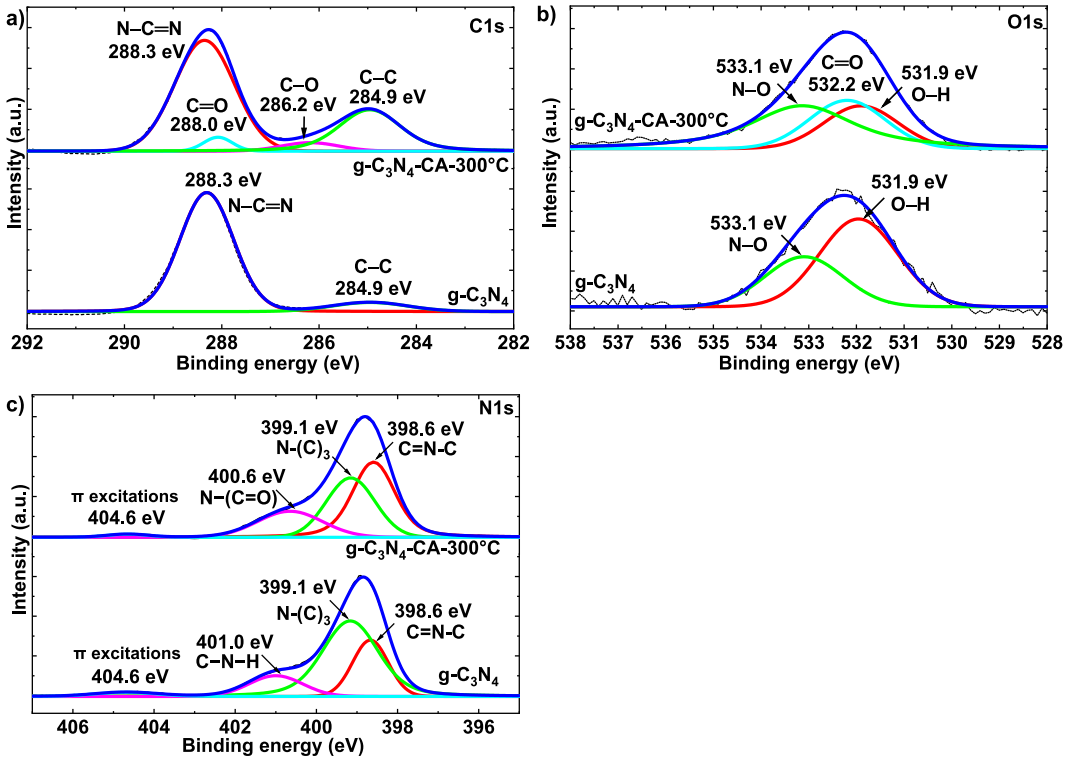

Fig. 5. XPS spectra of g-C_3N_4 and g-C_3N_4-CA-300 °C.

ring structure of g-C_3N_4. This indicated a chemical interaction between the citric acid and g-C_3N_4, which could potentially serve as a bridging mechanism for enhancing the charge transport.

The UV–vis absorption results demonstrated the tunability of the optical properties of the g-C_3N_4 and g-C_3N_4-CA. In Fig. 6**a**, the spectrum of g-C_3N_4 exhibited an absorption band in the range of 200–460 nm and in agreement with previous reports [52]. However, when the film was modified with citric acid and subjected to heat treatment, the absorption wavelength of g-C_3N_4-CA shifted towards higher wavelengths in range from 450 and 550 nm. Meanwhile, an absorption in the region of 600–800 nm was observed, indicating an improved visible light utilization ability. Additionally, the electronic structure of g-C_3N_4-CA might also have been altered due to the incorporation of citric acid and the thermal treatment process. These modifications have yielded diverse bandgap characteristics as shown in Fig. 6**b**. Specifically, the pristine g-C_3N_4 shows an energy bandgap of 2.84 eV, falling between the bandgap values of g-C_3N_4-CA without heating, which is 2.81 eV, and g-C_3N_4-CA at elevated temperatures. The g-C_3N_4-CA-200 °C and g-C_3N_4-CA-250 °C exhibited an equivalent bandgap of 2.83 eV. Conversely, g-C_3N_4-CA-300 °C and g-C_3N_4-CA-350 °C demonstrated wider bandgaps at 2.87 eV and 2.86 eV. However, the introduction of citric acid onto the g-C_3N_4 films slightly affected the energy bandgap. In **Fig. S4**, the UV–Vis spectra of g-C_3N_4 and g-C_3N_4-CA on the ITO glass were obtained at various citric acid (CA) concentrations after heating at 300 °C. As the results, the absorption wavelength of the heated g-C_3N_4-CA films slightly increased with the increase of the citric acid content compared to that observed for g-C_3N_4 on the ITO glass sample. Hence, the incorporation of citric acid into the g-C_3N_4 films has a negligible impact on their light absorption properties.

In Fig. 6**c**, The PL spectra showed the processes of charge migration, transfer, and separation in the films. The intensity of the emission peaks corresponds to the number of photons emitted at a specific energy. A higher photoluminescence emission peak indicates a higher rate of electron-hole pair recombination [53]. The obtained PL spectra showed that all samples, including the pure g-C_3N_4 and g-C_3N_4-CA samples, exhibited an emission within the range of 420–600 nm, which correlated with the 450-nm absorption edge of g-C_3N_4. However, a significant decrease in the PL intensity was observed in the g-C_3N_4-CA-300 °C sample compared to both the pure g-C_3N_4 and g-C_3N_4-CA sample. This observation aligns with the FTIR and XPS findings, suggesting that the NH—(C=O) bond serves as a bridge for carrier transfer and reduces the electron-hole recombination.

Heat treatment plays a crucial role in inducing a chemical interaction between the citric acid and g-C_3N_4, leading to robust adhesive films with improved mechanical properties. To assess this, g-C_3N_4 films, g-C_3N_4-CA films, and g-C_3N_4-CA films subjected to heat treatments at 200, 250, 300, and 350 °C were evaluated for their mechanical characteristics using manual removal by fingers. The results (**Fig. S5**) revealed that the pure g-C_3N_4 films exhibited an insufficient adhesion to the ITO glass, making them easily removed by the simple touch of a finger. In contrast, the other samples exhibited a strong adhesion, remaining firmly in place without any signs of detachment. Although the g-C_3N_4-CA films exhibited a strong adhesion, they experienced detachment from the ITO glass during photocurrent measurements in the Na_2SO_4 electrolyte system. The necessity for heat treatment arises from the inadequate curing at 120 °C to produce films with a robust adhesion. Thus, the g-C_3N_4-CA films were subjected to an additional heat treatment in the temperature range of 200–350 °C and showed an enhanced adhesion and stability during the measurements. Since iodine decomposes at temperatures between 50 and 140 °C [54], it would not affect g-C_3N_4 itself. However, the addition of citric acid (CA) and subsequent heat treatment would introduce hydroxyl-containing functional groups on the film, which would form chemical bonds with the functional groups on the ITO substrate and improve the adhesion of the g-C_3N_4 film. Moreover, the g-C_3N_4-CA film heated at 400 °C can be easily removed with

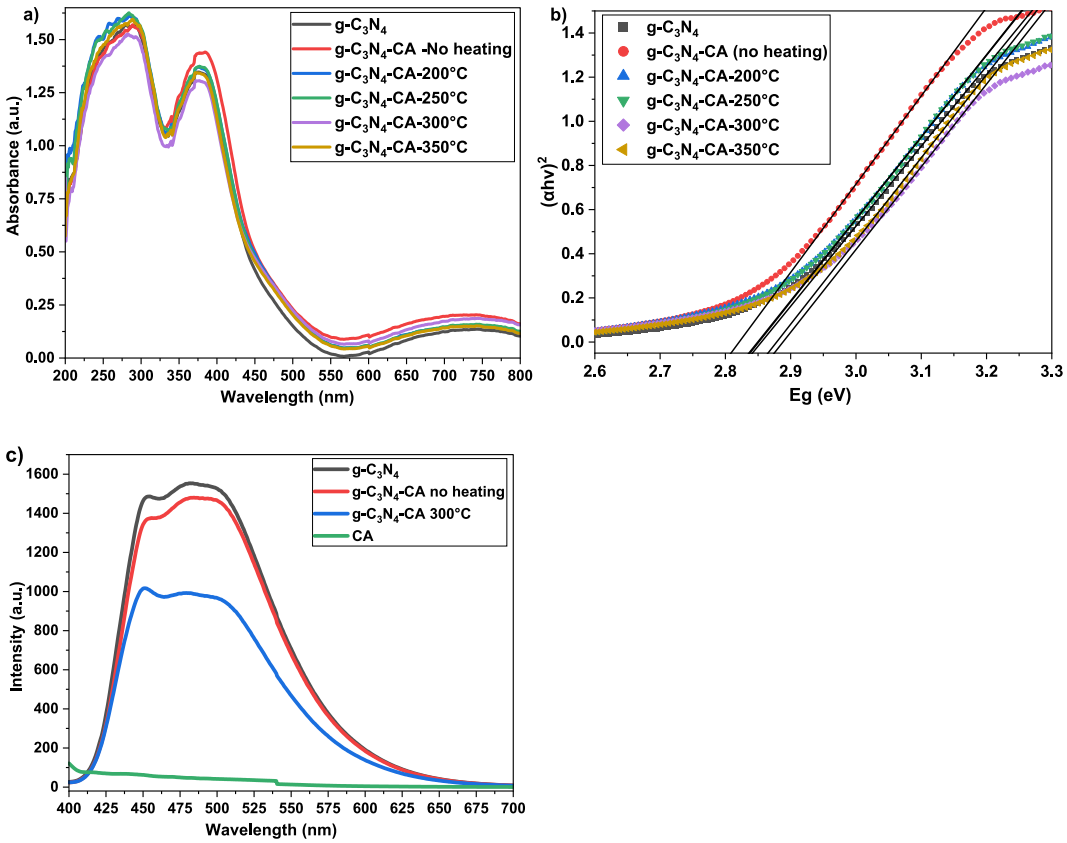

Fig. 6. UV–vis spectra of g-C_3N_4-CA on ITO glass obtained at a) different calcination temperatures, with a constant CA concentration of 75 g/l, b) band gap energy of the thin films and c) photoluminescence (PL) spectra of g-C_3N_4 and g-C_3N_4-CA on ITO glass before and after heating at 300 °C.

a gentle touch of a finger, and at 450 °C, all of the g-C_3N_4 and CA were burnt out and disappeared off the ITO glass.

The separation of electrons and holes was investigated by photocurrent measurements. When the films were exposed to a light source, there was a noticeable rise in the photocurrent. This increase is indicative of the migration of photo-generated electrons within the bulk materials, which consequently leads to the generation of the photocurrent during light irradiation. Fig. 7**a** shows the photocurrent response curves, while Fig. 7**b** displays the linear sweep voltammetry (LSV) plots of the prepared samples. The influence of the heat treatment temperature on the photocurrent response of the films was investigated at 200, 250, 300, and 350 °C. The results indicated that g-C_3N_4-CA heated at 300 °C exhibited the highest photocurrent response compared to the other temperatures. This suggests that a calcination temperature of 300 °C provided optimal conditions for efficient photocurrent generation in the citric acid-modified g-C_3N_4 film. This could be attributed to the robust physical properties and the strong crosslinking between CA and g-C_3N_4 through the NH— (C═O) bond, acting as a bridge for charge transport. Consequently, this can enhance the separation of electrons and holes, thereby contributing to improved photocurrent response characteristics. Fig. 7**c** shows that the rising time and decaying time of the photocurrent response are 0.18 and 0.2 s, respectively.

To investigate the influence of the citric acid concentration on the film stability, the g-C_3N_4 films were crosslinked with varying CA concentrations (10, 25, 50, 75, and 100 g/L), then heat-treated at 300 °C (Fig. S6**a**). Surprisingly, the films modified with CA at 10 g/L underwent cracking upon immersion in Na_2SO_4 electrolyte (Fig. S6**b**), implying inadequate crosslinking with g-C_3N_4 due to the low citric acid content. Conversely, g-C_3N_4 films modified with CA at concentrations of 25, 50, 75, and 100 g/L exhibited improved adhesion to the g-C_3N_4-ITO glass, preventing detachment during the photocurrent measurements. Photocurrent response curves (Fig. S7**a**) and linear sweep voltammetry (LSV) plots (Fig. S7**b**) revealed that at a 75 g/L CA concentration, the films exhibited the highest photocurrent response among the lower CA concentrations. This suggests the optimal citric acid concentration for maximizing the photocurrent in the g-C_3N_4-CA films. Notably, at the 100 g/L CA concentration, the photocurrent response exhibited a distinct shape, possibly due to excessive citric acid. This is supported by Fig. S6**a**, illustrating non-smooth and streaky film morphologies. The streaky appearance indicated incomplete integration of excess citric acid into the film matrix, resulting in uneven distribution and compromised film quality.

The investigation of charge transfer in the citric acid-modified g-C_3N_4 was conducted using electrochemical impedance spectra (EIS) (Fig. 7**d**), and the EIS parameters were obtained by fitting the experimental data with the equivalent circuit (**Fig. S8**). The observed trend in the semicircle diameters (g-C_3N_4-CA-250 °C > g-C_3N_4-CA-200 °C > g-C_3N_4-CA-350 °C > g-C_3N_4-CA-300 °C) signified variations in the conductivity, charge carrier migration efficiency, and electron-hole pair recombination [55]. Smaller diameters correspond to an enhanced conductivity, efficient charge transfer, and reduced recombination rate. Among the samples, g-C_3N_4-CA-300 °C exhibited the smallest semicircle diameter, suggesting that citric acid-modification and thermal treatment synergistically improved the conductivity, accelerated the charge transfer, and decreased the electron-hole recombination. The results support the investigation of the photocurrent response. The introduction of citric acid and heating is speculated to create C (acid) and N (g-C_3N_4) bonds with the NH_2 groups, fostering

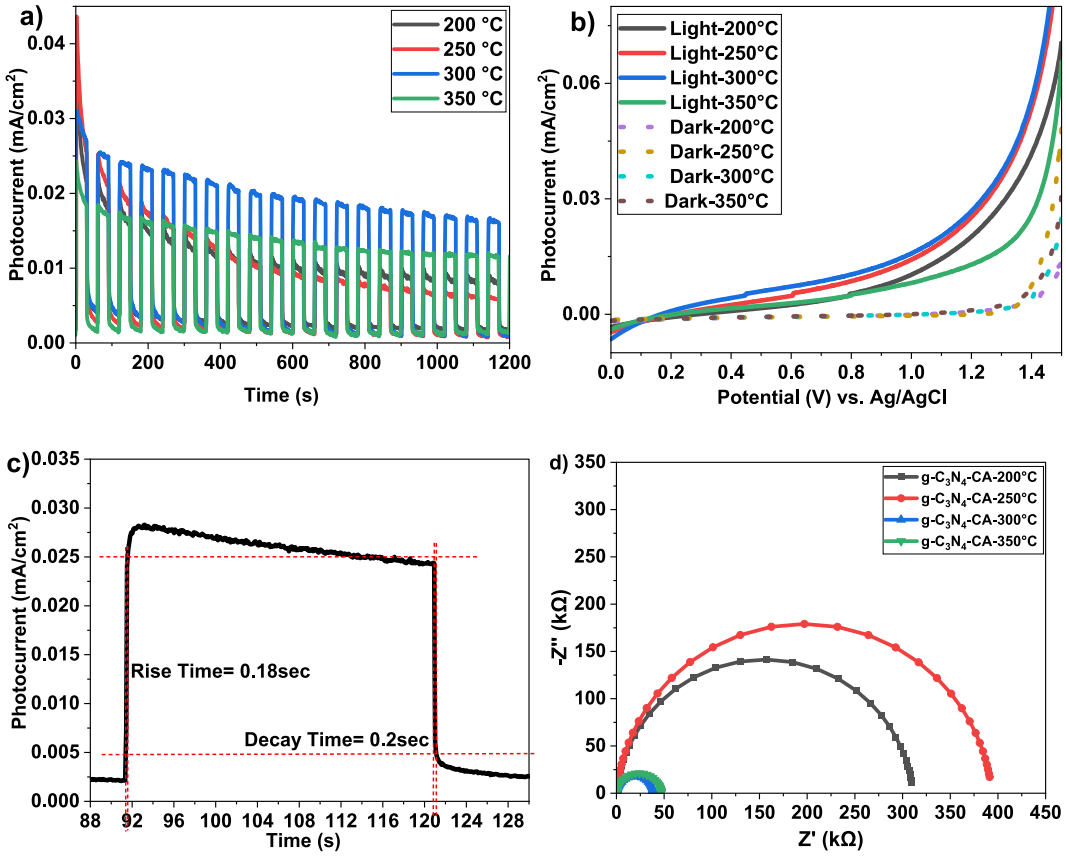

Fig. 7. A) photocurrent response, b)linear sweep voltammetry (LSV) plots of the films at different calcination temperatures, c) enlarged rising and decaying edges of the photocurrent response of the g-C_3N_4-CA-300 °C, and d) EIS Nyquist plots of citric acid-modified g-C_3N_4 films.

charge transfer and reducing recombination. Moreover, the hydrogen bonding between the compositions also speeds up the charge transfer. This modification is expected to facilitate efficient charge carrier migration, yielding higher photocurrents. In essence, this study highlights the impact of tailored citric acid modification and thermal treatment on the charge transfer properties within g-C_3N_4 with implications for an enhanced photocurrent response.

4. Conclusions

Citric acid-modified g-C_3N_4 films were successfully prepared, and the citric acid played a crucial role in enhancing the film stability and improving the photocurrent response. The modified samples exhibited a porous structure, optical absorption, reduced electron-hole recombination rates, and enhanced charge transfer, resulting in a high photocurrent response. Under optimal reaction conditions, the best sample, g-C_3N_4-CA-300 °C at a citric acid concentration of 75 g/L, achieved a photocurrent of approximately 0.025 mA/cm^2. This high photocurrent response can be primarily attributed to the strong adhesion, efficient transfer of the charge carriers and reduced electron-hole recombination. Therefore, citric acid-modified g-C_3N_4 holds significant promise as an environmentally-friendly material for various optoelectronic applications.

CRediT authorship contribution statement

Preyaphat Wongchaiya: Conceptualization, Data curation, Formal analysis, Investigation, Methodology, Validation, Visualization, Writing – original draft, Writing – review & editing. **Thi Kim Ngan Nguyen:** Conceptualization, Data curation, Formal analysis, Investigation, Methodology, Supervision, Validation, Visualization, Writing – original draft, Writing – review & editing. **Pornapa Sujaridworakun:** Conceptualization, Funding acquisition, Project administration, Resources, Software, Supervision, Writing – review & editing. **Siriporn Larpkiattaworn:** Conceptualization, Funding acquisition, Methodology, Project administration, Supervision, Writing – review & editing. **Tohru S. Suzuki:** Data curation, Resources, Software, Writing – review & editing. **Tetsuo Uchikoshi:** Conceptualization, Funding acquisition, Methodology, Project administration, Resources, Supervision, Writing – original draft, Writing – review & editing.

Declaration of competing interest

The authors declare that they have no known competing financial interests or personal relationships that could have appeared to influence the work reported in this paper.

Acknowledgements

The authors would like to thank Drs. M. Nemoto, İ. N. G. Özbilgin and T. Hiroto of National Institute for Materials Science (NIMS) for their help with the instrumental analyses. One of the authors, P. Wongchaiya, would like to express her deep gratitude to the following two institutions for supporting her research activities at NIMS through their educational programs: the Development and Promotion of Science and Technology Talents Project (DPST) Scholarship, Institute for the Promotion of Teaching Science and Technology (IPST), Ministry of Education, Thailand, and the International Cooperative Graduate Program (ICGP), NIMS, Japan.

Appendix A. Supplementary material

Supplementary data to this article can be found online at https://doi.org/10.1016/j.apt.2024.104460.

References

[1] S. Mokkapat, C. Jagadish, III-V compound SC for optoelectronic devices, Mater. Today 12 (2009) 22–32.
[2] X. Zhang, J. Shao, C. Yan, R. Qin, Z. Lu, H. Geng, T. Xu, L. Ju, A review on optoelectronic device applications of 2D transition metal carbides and nitrides, Mater. Des. 200 (2021) 109452.
[3] J. Yoon, S. Jo, I.S. Chun, I. Jung, H.-S. Kim, M. Meitl, E. Menard, X. Li, J.J. Coleman, U. Paik, J.A. Rogers, GaAs photovoltaics and optoelectronics using releasable multilayer epitaxial assemblies, Nature 465 (2010) 329–333.
[4] H.J. Joyce, Q. Gao, J. Wong-Leung, Y. Kim, H.H. Tan, C. Jagadish, Tailoring GaAs, InAs, and InGaAs nanowires for optoelectronic device applications, IEEE J. Sel. Top. Quantum Electron. 17 (2021) 766–778.
[5] J. Zhang, Y. Sun, S. Ye, J. Song, J. Qu, Heterostructures in Two-dimensional CdSe nanoplatelets:synthesis, optical properties, and applications, Chem. Mater. 32 (2020) 9490–9507.
[6] L. Gao, H. Chen, R. Wang, S. Wei, A.V. Kuklin, S. Mei, F. Zhang, Y. Zhang, X. Jiang, Z. Luo, S. Xu, H. Zhang, H. Ågren, Ultra-small 2D PbS nanoplatelets: Liquid-Phase exfoliation and emerging applications for photo-electrochemical photodetectors, Small 17 (2021) 2005913.
[7] S. Zhang, H. Jiao, X. Wang, Y. Chen, H. Wang, L. Zhu, W. Jiang, J. Liu, L. Sun, T. Lin, H. Shen, W. Hu, X. Meng, D. Pan, J. Wang, J. Zhao, J. Chu, Highly Sensitive InSb nanosheets infrared photodetector passivated by ferroelectric polymer, Adv. Funct. Mater. 30 (2020) 2006156.
[8] G. Dong, Y. Zhang, Q. Pan, J. Qiu, A fantastic graphitic carbon nitride (g-C3N4) material: electronic structure, photocatalytic and photoelectronic properties, J. Photochem. Photobiol. c: Photochem. Rev. 20 (2014) 33–50.
[9] K.R. Reddy, C.V. Reddy, S. Jaesool, T.M. Aminabhavi, M.N. Nadagouda, N.P. Shetti, Polymeric graphitic carbon nitride (g-C3N4)-based semiconducting nanostructured materials: synthesis methods, properties and photocatalytic applications, J. Environ. Manage. 238 (2019) 25–40.
[10] M. Sohail, U. Anwar, T. Taha, H. Qazi, A.G. Al-Sehemi, S. Ullah, H. Algarni, I. Ahmed, M.A. Amin, A. Palamanit, W. Iqbal, S. Alharthi, W. Nawawi, Z. Ajmal, H. Ali, A. Hayat, Nanostructured materials based on g-C_3N_4 for enhanced photocatalytic activity and potentials application: A review, Arab. J. Chem. 15 (2022) 104070.
[11] T.R. Chetia, M.S. Ansari, M. Qureshi, Graphitic carbon nitride as a photovoltaic booster in quantum dot sensitized solar cells: a synergistic approach for enhanced charge separation and injection, J. Mater. Chem. A 4 (2016) 5528–5541.
[12] Z. Cai, J. Chen, S. Xing, D. Zheng, L. Guo, Highly fluorescent g-C_3N_4 nanobelts derived from bulk g-C_3N_4 for NO_2 gas sensing, J. Hazard. Mater. 416 (2021) 126195.
[13] Y. Luo, Y. Yan, S. Zheng, H. Xue, H. Pang, Graphitic carbon nitride based materials for electrochemical energy storage, J. Mater. Chem. A 7 (2019) 901–924.
[14] W.-J. Ong, L.-L. Tan, Y.H. Ng, S.-T. Yong, S.-P. Chai, Graphitic carbon nitride (g-C3N4)-based photocatalysts for artificial photosynthesis and environmental remediation: are we a step closer to achieving sustainability?, Chem Rev. 116 (2016) 7159–7329.
[15] Z. Yang, Y. Zhang, Z. Schnepp, Soft and hard templating of graphitic carbon nitride, J. Mater. Chem. A 3 (2015) 14081–14092.
[16] L. Jiang, X. Yuan, Y. Pan, J. Liang, G. Zeng, Z. Wu, H. Wang, Doping of graphitic carbon nitride for photocatalysis: A review, Appl. Catal. b: Environ. 217 (2017) 388–406.
[17] Z. Zhao, Y. Suna, F. Dong, Graphitic carbon nitride based nanocomposites: a review, Nanoscale 7 (2015) 15–37.
[18] M. Majdoub, Z. Anfar, A. Amedlous, Emerging chemical functionalization of g-C_3N_4: covalent/noncovalent modifications and applications, ACS Nano 14 (2020) 12390–12469.
[19] D. Vidyasagar, S.G. Ghugal, S.S. Umare, M. Banavoth, Extended π-conjugative n-p type homostructural graphitic carbon nitride for photodegradation and charge-storage applications, Sci. Rep. 9 (2019) 7186.
[20] J. Xu, L. Zhang, R. Shi, Y. Zhu, Chemical exfoliation of graphitic carbon nitride for efficient heterogeneous photocatalysis, J. Mater. Chem. A 1 (2013) 14766–14772.
[21] X. Wang, L. Wu, Z. Wang, H. Wu, X. Zhou, H. Ma, H. Zhong, Z. Xing, G. Cai, C. Jiang, F. Ren, C/N vacancy co-enhanced visible-light-driven hydrogen evolution of g-C3N4 nanosheets through controlled He+ ion irradiation, Sol. RRL 3 (2019) 1800298.
[22] J. Safaei, N.A. Mohamed, M.F.M. Noh, M.F. Soh, M.A. Riza, N.S.M. Mustakim, N. A. Ludin, M.A. Ibrahim, W.N.R.W. Isahak, M.A.M. Teridi, Facile fabrication of graphitic carbon nitride, (g-C3N4) thin film, J. Alloys Compd. 769 (2018) 130–135.
[23] E.B. Chubenko, N.G. Kovalchuk, I.V. Komissarov, V.E. Borisenko, Chemical vapor deposition of 2D crystallized g C_3N_4 layered films, J. Phys. Chem. C 126 (2022) 4710–4714.
[24] N. Li, Y. Tian, J. Zhao, J. Zhang, W. Zuo, L. Kong, H. Cui, Z-scheme 2D/3D g-C_3N_4@ZnO with enhanced photocatalytic activity for cephalexin oxidation under solar light, Chem. Eng. J. 352 (2018) 412–422.
[25] S. Obregón, G. Amor, A. Vázquez, Electrophoretic deposition of photocatalytic materials, Adv. Colloid Interface Sci. 269 (2019) 236–255.
[26] D. Han, J. Liu, H. Cai, X. Zhou, L. Kong, J. Wang, H. Shi, Q. Guo, X. Fan, High-yield and low-cost method to synthesize large-area porous g-C_3N_4 nanosheets with improved photocatalytic activity for gaseous nitric oxide and 2-propanol photodegradation,", Appl. Surf. Sci. 464 (2019) 577–585.
[27] B. L. Phoon, J. M. b. Husin, K.-C. Lee, B. F. Leo, T. C.-K. Yang, C. W. Lai and J. C. Juan, Crystallinity and lattice vacancies of different mesoporous g-C_3N_4 for photodegradation of tetracycline and its cytotoxic implication, Chemosphere 308 (2022) 136219.
[28] Y. Dong, Y. Chen, P. Jiang, G. Wang, X. Wu, R. Wu, A novel g-C_3N_4 based photocathode for photoelectrochemical hydrogen evolution, RSC Adv. 6 (2016) 7465–7473.
[29] J. Xu, M. Shalom, Electrophoretic deposition of carbon nitride layers for photoelectrochemical applications, ACS Appl. Mater. Interfaces 8 (2016) 13058–13063.
[30] B. Wang, H. Cai, D. Zhao, M. Song, P. Guo, S. Shen, D. Li, S. Yang, Enhanced photocatalytic hydrogen evolution by partially replaced corner-site C atom with P in g-C_3N_4, Appl. Catal. b: Environ. 244 (2019) 486–493.
[31] R. Salihu, S.I.A. Razak, N.A. Zawawi, M.R.A. Kadir, N.I. Ismail, N. Jusoh, M.R. Mohamad, N.H.M. Nayan, Citric acid: A green cross-linker of biomaterials for biomedical applications, Eur. Polym. J. 146 (2021) 110271.
[32] R. Ciriminna, F. Meneguzzo, R. Delisi, M. Pagliaro, Citric acid: emerging applications of key biotechnology industrial product, Chem. Cent. J. 11 (2017) 22.
[33] V. Mikelashvili, S. Kekutia, J. Markhulia, L. Saneblidze, N. Maisuradze, M. Kriechbaum, L. Almásy, Synthesis and characterization of citric acid-modified iron oxide nanoparticles prepared with electrohydraulic discharge treatment, Materials 16 (2023) 746.
[34] S. Shinohara, N. Eom, E.-J. Teh, K. Tamada, D. Parsons, V.S.J. Craig, The role of citric acid in the stabilization of nanoparticles and colloidal particles in the environment: measurement of surface forces between hafnium oxide surfaces in the presence of citric acid, Langmuir 34 (2018) 2595–2605.
[35] X. Cui, A. Ozaki, T.-A. Asoh, H. Uyama, Cellulose modified by citric acid reinforced Poly(lactic acid) resin as fillers, Polym. Degrad. Stab. 175 (2020) 109118.
[36] N. Reddy, Y. Yang, Citric acid cross-linking of starch films, Food Chem. 118 (2010) 702–711.
[37] S.H. Lee, P.M. Tahir, W.C. Lum, L.P. Tan, P. Bawon, B.-D. Park, S.S.O.A. Edrus, U.H. Abdullah, A review on citric acid as green modifying agent and binder for wood, Polym. 12 (2020) 1692.
[38] L. Vallan, H. Imahori, Citric acid-based carbon dots and their application in energy conversion, ACS Appl. Electron. Mater. 4 (2022) 4231–4257.
[39] T. Narkbuakaew, P. Sujaridworakun, Synthesis of Tri-S-Triazine Based g-C_3N_4 Photocatalyst for Cationic Rhodamine B Degradation under Visible Light, Top. Catal. 63 (2020) 1086–1096.
[40] A. Sulthan Ibrahim, K.V. Alex, M.B. Latha, K. Kamakshi, S. Sathish, J.P.B. Silva, K. C. Sekhar, Effect of the thickness on the photocatalytic and the photocurrent properties of ZnO films deposited by spray pyrolysis, Discov. Mater. 2 (2022) 10.
[41] X. Wang, K. Maeda, A. Thomas, K. Takanabe, G. Xin, J.M. Carlsson, K. Domen, M. Antonietti, A metal-free polymeric photocatalyst for hydrogen production from water under visible light, Nat. Mater. 8 (2009) 76–80.
[42] P. Wiecinska, Thermal degradation of organic additives used in colloidal shaping of ceramics investigated by the coupled DTA/TG/MS analysis, J. Therm. Anal. Calorim. 123 (2016) 1419–1430.
[43] D. Wyrzykowski, E. Hebanowska, G. Nowak-Wiczk, M. Makowski, L. Chmurzyński, Thermal behaviour of citric acid and isomeric aconitic acids, J. Therm. Anal. Calorim. 104 (2011) 731–735.
[44] M.M. Barbooti, D.A. Al-sammerrai, Thermal decomposition of citric acid, Thermochim. Acta 98 (1986) 119–126.
[45] F. Dong, Z. Zhao, T. Xiong, Z. Ni, W. Zhang, Y. Sun, W.-K. Ho, In Situ Construction of g-C_3N_4/g-C_3N_4 metal-free heterojunction for enhanced visible-light photocatalysis, ACS Appl. Mater. Interfaces 5 (2013) 11392–11401.
[46] B. Zhu, P. Xia, W. Ho, J. Yu, Isoelectric point and adsorption activity of porous g-C_3N_4, Appl. Surf. Sci. 344 (2015) 188–195.
[47] R. Ludmerczki, S. Mura, C.M. Carbonaro, I.M. Mandity, M. Carraro, N. Senes, S. Garroni, G. Granozzi, L. Calvillo, S. Marras, L. Malfatti, P. Innocenzi, Carbon dots from citric acid and its intermediates formed by thermal decomposition, Chem.–A Euro J. 25 (2019) 11963–11974.
[48] L. Shen, Z. Xing, J. Zou, Z. Li, X. Wu, Y. Zhang, Q. Zhu, S. Yang, W. Zhou, Black TiO_2 nanobelts/g-C_3N_4 nanosheets laminated heterojunctions with efficient visible-light- driven photocatalytic performance, Sci. Rep. 7 (2017) 41978.
[49] Y. Ding, F. Zhang, J. Xu, Y. Miao, Y. Yang, X. Liu, B. Xu, Synthesis of short-chain passivated carbon quantum dots as the light emitting layer towards electroluminescence, RSC Adv. 7 (2017) 28754–28762.
[50] L. Jia, X. Cheng, X. Wang, H. Cai, P. He, J. Ma, L. Li, Y. Ding, X. Fan, Large-scale preparation of g C_3N_4 porous nanotubes with enhanced photocatalytic activity by using salicylic acid and melamine, Ind. Eng. Chem. Res. 59 (2020) 1065–1072.

[51] Y. Zhao, H. Qin, Z. Wang, H. Wang, Y. He, Q. Tian, Q. Luo, P. Xu, Facile synthesis of cadmium doped graphite carbon nitride for photocatalytic degradation of tetracycline under visible light irradiation, Environ. Sci. Pollut. Res. 29 (2022) 74062–74080.
[52] G. Zhang, T. Zhang, B. Li, S. Jiang, X. Zhang, L. Hai, X. Chen, W. Wu, An ingenious strategy of preparing TiO_2/g-C_3N_4 heterojunction photocatalyst: In situ growth of TiO_2 nanocrystals on g-C_3N_4 nanosheets via impregnation-calcination method, Appl. Surf. Sci. 433 (2018) 963–974.
[53] Z. Yang, K. Hu, X. Meng, Q. Tao, J. Dong, B. Liu, Q. Lu, H. Zhang, B. Sundqvist, P. Zhu, M. Yao and B. b. Liu, Tuning the band gap and the nitrogen content in carbon nitride materials by high temperature treatment at high pressure, Carbon 130 (2018) 170-177.
[54] Q. Zhang, Z. Wu, F. Liu, S. Liu, J. Liu, Y. Wang, T. Yan, Encapsulating a high content of iodine into an active graphene substrate as a cathode material for high-rate lithium–iodine batteries, J. Mater. Chem. A 5 (2017) 15235–15242.
[55] S.J. Hong, S. Lee, J.S. Jang, J.S. Lee, Heterojunction $BiVO_4$/WO_3 electrodes for enhanced photoactivity of water oxidation, Energy Environ. Sci. 4 (2011) 1781–1787.